The Effect of Micro-structural Mechanisms on the Macro-level Behaviour of Cementitious Materials at Elevated Temperatures

Jiayi Wang[1], Colin T Davie[1,*], Enrico Masoero[1]

[1]School of Engineering, Newcastle University

Newcastle upon Tyne, United Kingdom

* Colin T Davie (colin.davie@ncl.ac.uk, Drummond Building, Newcastle University, Newcastle upon Tyne, NE1 7RU)

ABSTRACT

The benchmark problem [1] presented by Wang et al. [2] has been further explored to consider the effect of micro-structural mechanisms on the macro-level behaviour of concrete at elevated temperatures, again using an existing fully coupled, hygro-thermo-mechanical model [3] cast in a finite element framework and implemented in the research code FEAP [4]. Results relating to the evolution of temperature and gas pressure are presented. Early investigations and previous works have confirmed that intrinsic permeability and its evolution with temperature is key to the development of gas pressures [2, 5]. Additionally, the amount of water introduced into the system as a result of dehydration of the cement paste, the influence of micro-scale gas flow behaviour and the evolution of capillary pressures are investigated and all found to have considerable effect on the development of macro-scale behaviours. Further work will consider more specifically the evolution of the pore size distribution, its relationship to dehydration and its effect on macro-scale material properties such as porosity, permeability and sorption isotherms.

KEYWORD: concrete, micro-structural, high temperature, numerical model, dehydration, gas slip, capillary pressure

INTRODUCTION

Spalling is one of the most severe failure modes for concrete under high temperature yet there remains no concensus on the underlying causes of spalling with two main theories tying it to thermally induced stresses [6, 7] or the developed of internal pore pressures [8, 9]. Whatever the cause, it is hypothesised here that many of the behaviours observed at the macro-scale in concrete exposed to elevated temperatures are in fact a function of behaviour occurring at the micro-scale within the porous micro-structure of the material. However, due to the complexity of the coupled hygro-thermo-chemo-mechanical behaviours that occur in cementitious materials when heated, the effect on macro-scale behaviour of processes occurring at the micro-scale and the evolution of the micro-structure itself with temperature is not holistically understood. Concrete is a multi-phase material and the mechanical characteristics of concrete at high temperatures are not only determined by those components within it but also associated with its intrinsic properties, such as

permeability, porosity, thermal conductivity and strength [3] all of which can be related to the micro-structure. Most of these intrinsic characteristic properties are seen to be temperature dependent when measured empirically at the macro-scale. However, fundamentally, all of these properties and their temperature dependence should be relatable to the micro-struture of the material and its evolution with temperature. For example, porosity is a direct measure of the micro-structural space within the cementitious structure and controls the limits of fluid content in the material. Permeability and diffusivity are functions of the connectivity of that space and contol the transport of fluids through the material. Dehydration of the cement paste during heating releases water into the pore space, affecting overall transport behaviour and energy balance, and in doing so leads to changes in the pore structure and the pore sizes and hence changes the porosity, permeability and diffusivity. In turn, those micro-structural changes will affect the development of capillary menisci, thus affecting the water/vapour equilibrium (sorption isotherms) for the material [5].

To investigate some of these micro-structural influences a fully coupled hygro-thermo-mechanical model for concrete originally developed by Davie *et al.* [3] has been employed. The model is cast in a finite element framework and implemented in the research code FEAP [4]. The complex behaviours of concrete are captured through the adoption of multi-phase material descriptions which represent strong coupled behaviours of solid, liquid and gas phases which are considered separately [3]. The model has been employed here to reproduce the results of the benchmark tests [1] (specifically temperatures and gas pressures) and explore the effects of several micro-structural behaviours. These are namely, variation in the quantities of water derived through dehydration, the influence of Klinkenberg gas-slip effects [8] and the evolution of capillary pressure with water contents, which is related to pore size distribution. (It should be made clear that, at this stage, spalling is not explicitly considered). By tuning of macro-scale properties and modifing modelling assumptions, insight can be gained into the influence of key factors in controlling the observed experimental results which in turn help to identify avenues for further research.

MATHEMATICAL MODEL

The fully coupled hygro-thermo-mechanical model considers concrete as a multi-phase material consisting of solid (cementitious skeleton), liquid (free water) and gas (water vapour and dry air) phases and solves for the primary variables of temperature, gas pressure and vapour content. The concrete is considered to behave elastically with the degradation of the material due to both mechanical and thermal loading accounted for via an isotropic thermo-mechanical damage formulation. The liquid phase is subject to Darcian pressure driven flow while the gas phase (considered as a mixture of ideal gases) is subject to both Fickian diffusion and pressure driven flow. Evaporation and condensation of the liquid water and vapour are possible and dehydration of water from the solid skeleton is also considered. Coupling between the fluid and solid phases is achieved via a Bishop-type effective stress approach. The governing conservative, fluid transport and mechanical strain equations of the model are briefly described below while the full details of the formulations and implementations with auxiliary functions are presented in Davie *et al.* [3].

Governing Conservative Equations

The model consists of four governing equations: mass conservation of dry air (1), mass conservation of moisture (inc. water vapour and liquid water) (2), energy conservative equation (3) and linear momentum balance (4):

$$\frac{(\varepsilon_G \tilde{\rho}_A)}{\partial t} = -\nabla \cdot \mathbf{J}_A \tag{1}$$

$$\frac{(\varepsilon_G \tilde{\rho}_V)}{\partial t} + \frac{(\varepsilon_L \rho_L)}{\partial t} - \frac{(\varepsilon_D \rho_L)}{\partial t} = -\nabla \cdot (\mathbf{J}_V + \mathbf{J}_L) \tag{2}$$

$$\left(\underline{\rho C}\right)\frac{\partial T}{\partial t} - \lambda_E \frac{\partial(\varepsilon_L \rho_L)}{\partial t} + (\lambda_D + \lambda_E)\frac{(\varepsilon_D \rho_L)}{\partial t} = -\nabla \cdot (k \nabla T) + \lambda_E \nabla \cdot \mathbf{J}_L \tag{3}$$

$$\nabla \cdot (\sigma' - \eta P_{Pore}\mathbf{I}) + \mathbf{b} = 0 \tag{4}$$

where, ε_θ is the volume fraction of a phase θ ($\theta = L, V, A, G, D$ refer to liquid water, water vapour, dry air, gas mixture and dehydrated water phases, respectively), ρ_θ is the density of a phase θ, $\tilde{\rho}_\theta$ the mass of a phase θ per unit volume of gaseous material, $\mathbf{J}_\theta$ the mass flux of a phase θ, $\underline{\rho C}$ the heat capacity of concrete, k the effective thermal conductivity of concrete, λ_D is the specific heat of dehydration, λ_E is the specific heat of evaporation (or of desorption), T is the temperature, $\boldsymbol{\sigma}'$ is the Bishop's stress, $\mathbf{I}$ is the identity matrix, η is the Biot coefficient, P_{Pore} is the pore pressure, $\mathbf{b}$ is the body force and t is time [3].

Fluid Transport Equations

Transport of the liquid water phase is described by Darcy's law where the water is assumed to flow through the pore structure of concrete under pressure, while the concentration driven the diffusion of the gas phase is assumed to obey the Fick's law. The mass fluxes of water vapour, dry air and liquid water per unit area of concrete are then given respectively by:

$$\mathbf{J}_A = \varepsilon_G \tilde{\rho}_A(\mathbf{v}_G) - \varepsilon_G \tilde{\rho}_G D_{AV} \nabla\left(\frac{\tilde{\rho}_A}{\tilde{\rho}_G}\right) \tag{5}$$

$$\mathbf{J}_V = \varepsilon_G \tilde{\rho}_V(\mathbf{v}_G) - \varepsilon_G \tilde{\rho}_G D_{AV} \nabla\left(\frac{\tilde{\rho}_V}{\tilde{\rho}_G}\right) \tag{6}$$

$$\mathbf{J}_L = \varepsilon_L \rho_L(\mathbf{v}_L) \tag{7}$$

where, D_{AV} is the coefficient of diffusion for the dry air/water vapour mixture within the porous concrete and $\mathbf{v}_G$ & $\mathbf{v}_L$ are the Darcian velocities of the gas and liquid water phases, given by:

$$\mathbf{v}_G = -\frac{k_g K \cdot K_G}{\mu_G} \nabla P_G \qquad \mathbf{v}_L = -\frac{K \cdot K_G}{\mu_G} \nabla P_L \tag{8}$$

where K is the intrinsic permeability of the concrete, K_θ, μ_θ and P_θ are the relative permeability, dynamic viscosity and pressure of the phase θ and k_g is the gas-slip factor, given by:

$$k_g = \left(1 + \frac{b \cdot P_{Atm}}{P_G}\right), \text{ with } b = e^{(-0.5818 \ln(K) - 19.1213)} \tag{9}$$

where, P_{Atm}=101325 Pa is standard atmospheric pressure and b is the Klinkenberg gas-slip flow constant [8].

The relative permeabilities that describe the variations in flow induced by the partial content of gas and liquid phases in the concrete pore spaces and are defined by [3]:

$$K_G = 10^{S\lambda} - 10^{\lambda} S \qquad K_L = 10^{(1-S)\lambda} - 10^{\lambda}(1 - S) \tag{10}$$

Where, S is the degree of liquid water saturation and λ is a function of porosity, ϕ.

$$S = \frac{\varepsilon_L}{\phi} \qquad \lambda = 0.05 - 22.5\phi \tag{11}$$

Capillary suctions are considered by way of the Kelvin equation:

$$P_L = P_G - P_C, \text{ with } P_C = \begin{cases} -R_V T \rho_L \ln\left(\frac{P_V}{P_{Sat}}\right) & \text{for } S > S_{SSP} \\ 0 & \text{for } S \leq S_{SSP} \end{cases} \tag{12}$$

where, R_V is the ideal gas constant of water vapour [12], P_V is the vapour pressure and P_{Sat} is the water vapour saturation pressure. S_{SSP} is the solid saturation point, below which all water is assumed to exist as adsorbed water, physically bound to the concrete skeleton [8] and so capillary menisci cannot form.

Ideal gas behaviour is assumed for the dry air and water vapour:

$$P_A = R_A \tilde{\rho}_A T \qquad P_V = R_V \tilde{\rho}_V T \tag{13}$$

and their partial pressures and densities are assumed to obey Dalton's law of additivity [12]:

$$P_G = P_A + P_V \qquad \tilde{\rho}_G = \tilde{\rho}_A + \tilde{\rho}_V \tag{14}$$

The saturation with liquid water (and hence the volume fraction of liquid water (11)) in the concrete is calculated by the sorption isotherms:

$$S = f(A, B(T), h) \tag{15}$$

where, *A* is a set of material constants, *B*(*T*) is a set of temperature dependent material properties and *h* is the relative humidity. The volume fraction of gas, ε_G, is calculated by:

$$\phi = \varepsilon_L + \varepsilon_G \tag{16}$$

Detailed functions for the material parameters employed in the formulation above are presented in [2, 9].

Mechanical Formulation

As mentioned above, the model has a fully coupled hygro-thermal-mechanical formulation, however the mechanical behaviour is not explicitly considered here and so for brevity the mechanical component is omitted. The detailed formulation is presented in [2, 9].

Boundary Conditions

Heat transfer across the boundary is described by:

$$\frac{\partial T}{\partial n} = \frac{h_{qr}}{K_{TT}}\left(T_{\infty} - T\right) \tag{17}$$

where T_∞ is the atmospheric temperature and h_{qr} is the sum of radiation and convection heat transfer coefficients on the boundary. It is assumed that the boundary is dry and no liquid water flux occurs [12] so only water vapour transfer is considered:

$$\frac{\partial \tilde{\rho}_v}{\partial n} = -\frac{K_{VT} h_{qr}}{K_{VV} k}\left(T_{\infty} - T\right) + \frac{\beta}{K_{VV}}\left(\tilde{\rho}_{V,\infty} - \tilde{\rho}_V\right) \tag{18}$$

where, β is the coefficient of water vapour mass transfer on the boundary and $\tilde{\rho}_{V,\infty}$ is the vapour content in the atmosphere. (Full formulations for the terms K_{TT}, K_{VT} & K_{VV} can be found in [3]).The gas pressure on the boundary is given by:

$$P_G = P_{G,\infty} \tag{19}$$

NUMERICAL ANALYSES

The model set up for this high-temperature problem, representative of concrete slabs 120mm thick and 300 × 300mm in plan area subjected to different heating scenarios on one face, is shown in Figure 1. For simplicity, a 1D approach is adopted in the first instance.

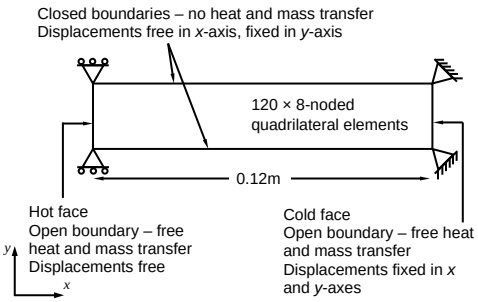

Figure 1 One-dimensional model set up.

The model was employed to reproduce as closely as possible the experimental heating scenario where the temperature in the atmosphere was raised instantly to 600°C and held

constant throughout the test. The key material parameters and the initial internal conditions of the three types of concrete were provided from the [1] and [13] and are shown in Table 1. In [3], the model was set up using these parameter values in order to directly compare the model prediction to the experimental results. These results are here used as a benchmark to study the influence of the various micro-scale mechanisms described above.

Table 1 Initial conditions and material properties for two concrete types.

Parameter	Initial conditions and material properties	
	B40	**B60**
Initial internal temperature	20°C	20°C
Initial internal gas pressure	101325Pa	101325Pa
Initial internal vapour content	0.0074336 kg/m^3 ≡ ~43% RH	0.0134842 kg/m^3 ≡ ~78% RH
Initial porosity	13.85%	10.55%
Initial permeability, K_0	1.0×10^{-19} m^2 (@20°C)	6.0×10^{-20} m^2 (@20°C)
Bulk density	2285 kg/m^3	2364 kg/m^3
Solid density	2583 kg/m^3	2551 kg/m^3
Young's modulus	24 GPa	39 GPa
Poisson's ratio	0.2	0.2
Compressive strength	30 MPa	67 MPa
Tensile strength	2.4 MPa	3.8 MPa

The boundary heat transfer properties for these analyses were taken from previous work [3], which in turn followed the work of [14], looking at the experiments of [13].

RESULTS

Analysis 1 – Permeability: As presented in Wang et al.[2], the initial permeability was adjusted by trial and error until a good match was reached between the numerical and experimental gas pressure peaks. Results of gas pressure and temperature are given in Figure 2a-d with the numerical permeability indicated on the right.

(Experimental K_0: B40 - 5.53×10^{-16} m^2; B60 - 1.67×10^{-16} m^2).

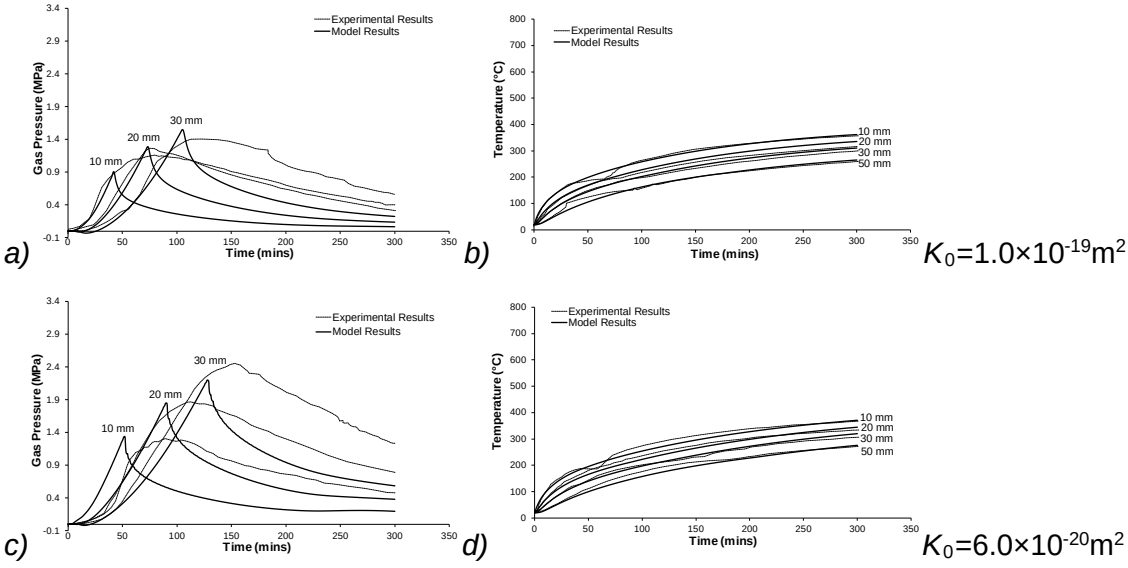

Figure 2 Numerical and experimental results showing gas pressures (left) (tuned via permeability) and temperatures (right) with time for a) & b) B40, c) & d) B60

As discussed in [2], firstly, it can be seen that the temperature profiles are matched reasonably well in all cases with only slight differences in the early stages. Secondly, the gas pressure peak heights and their evolution with depth and time can be matched reasonably well in all cases however the shape of the experimental peaks are quite rounded and

elongate under moderate heating whereas the model predicts sharp peaks. It should also be noted that the permeabilities applied in the model are several orders of magnitude smaller than those measured experimentally (~2 for B40; ~4 for B60). It is well known that the intrinsic permeability plays a great role in controlling gas pressure development [12, 15,16] but other factors including the amount of moisture introduced into the system, differences in gas and liquid transport behaviour and capillary suctions may also be significant. *Analysis 2 - 5* explore these issues further.

Analysis 2 – Volume of water released by dehydration

Independent of the permeability, the moisture content within the concrete has a significant effect on the development of gas pressures. The moisture content is not only determined by the initial saturation (the volume of free water within the microstructure before heating starts) but is also related to the amount water released by dehydration of the cement paste upon exposure to high-temperatures. Figure 3a shows the dehydration function described by:

$$\varepsilon_D \rho_L = \begin{cases} 0 & for\ (T_c \leq 200℃) \\ a(f_{rec})T_c^3 + b(f_{rec})T_c^2 + c(f_{rec})T_c + d & for\ (200℃ < T_c \leq 300℃) \\ 0.4 \times 10^{-4}\rho_c(T_c - 300) + (f_{rec} - 0.02)\rho_c & for\ (300℃ < T_c \leq 800℃) \\ f_{rec}\rho_c & for\ (T_c > 800℃) \end{cases} \quad (20)$$

where ρ_c is the volume fraction of cement paste in the concrete mix, f_{rec} = 0.09 is the fraction of cement paste that is recoverable as water and *a*,*b*,*c*,and *d* are coefficients of a cubic function (and functions of f_{rec}) such that $\varepsilon_D \rho_L(T)$ and its derivative, $\partial \varepsilon_D \rho_L / \partial T$ are continuous. This function, employed in the model used here [3], was adapted from [12] who cites [17, 18] as its source. Upon inspection of (12) it may be noted that for the concretes employed in the benchmark problem, where ρ_c = 300 kg/m^3, the f_{rec} = 0.09 fraction given by [12] produces a maximum volume of water from dehydration of 27 kg/m^3, making it a secondary source of water compared to the initial free water content. It may also be noted that this volume is significantly less than the volumes of water resulting from dehydration suggested by [15, 16].

To investgate the significance of this source of water into the coupled system, equation (21) was modified using two larger fractions of cement content (f_{rec} = 0.4 & f_{rec} = 0.6). These are shown in Figure 3b and result in maximum volumes of 120 kg/m^3 and 180 kg/m^3 of water from dehydration respectively.

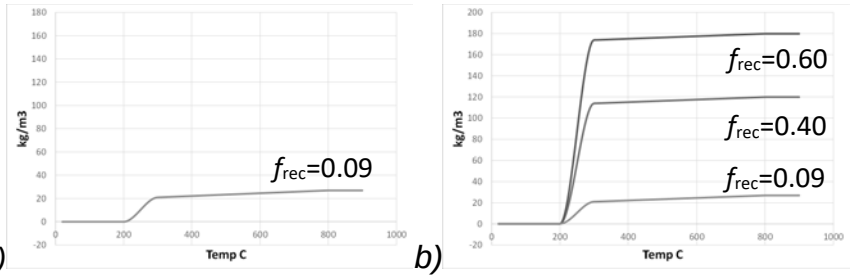

a) *b)*

Figure 3 Mass of water released by dehydration with temperature for *a)* original dehydration function, *b)* increased dehydration functions

The benchmark analyses conducted in *Analysis 1* were repeated using the same permeabilities and applying these two new curves. Results of gas pressure and temperature are shown in Figure 4a-h.

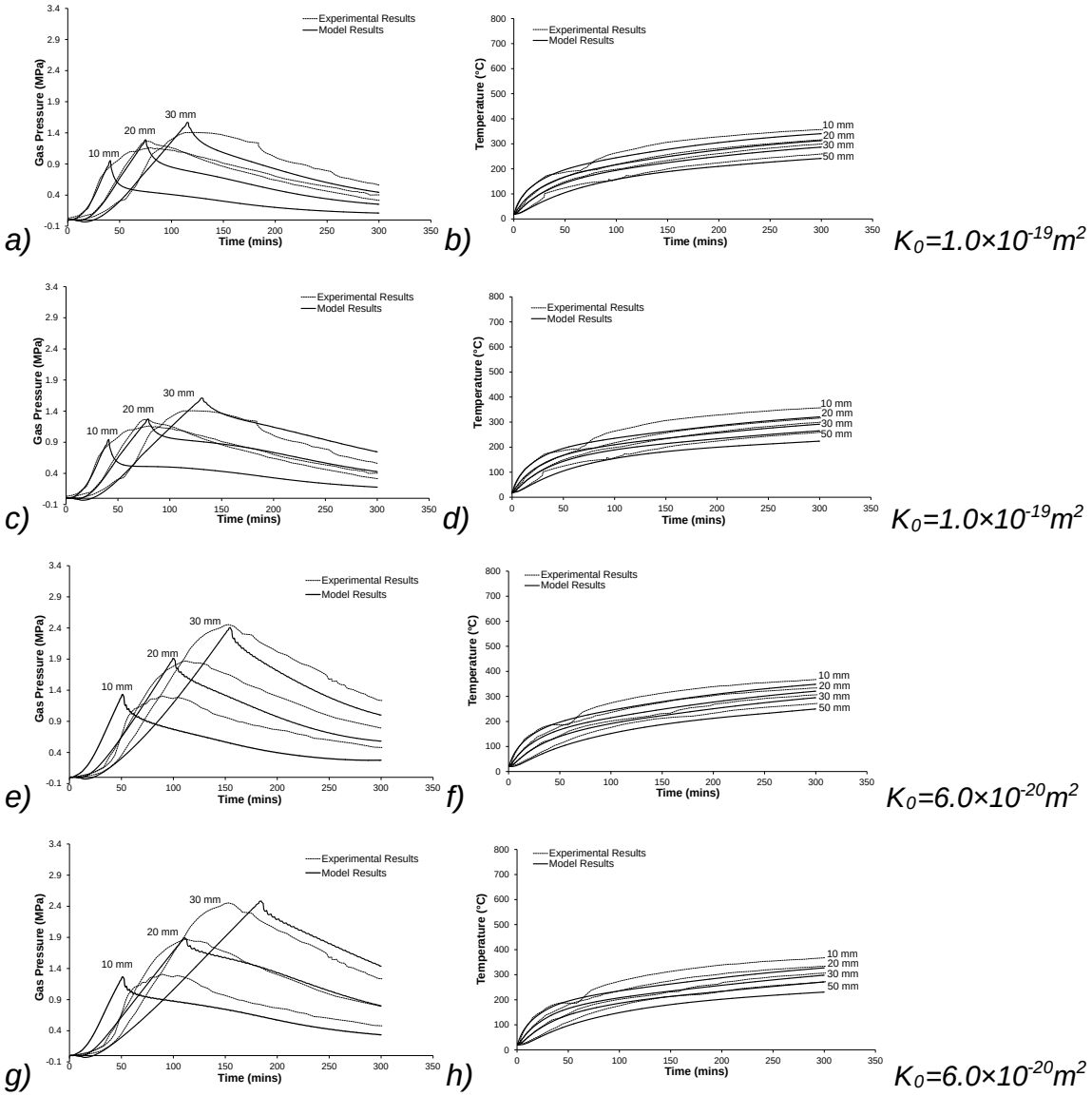

Figure 4 Numerical and experimental results showing gas pressures (left) and temperatures (right) in time for a) & b) B40 with f_{rec}=0.4, c) & d) B40 with f_{rec}=0.6, e) & f) B60 with f_{rec}=0.4 , g) & h) B60 with f_{rec}=0.6

From examination of these results and comparison with results in Figure 2 several things should be noted. Firstly, although the height of the gas pressure peaks has not changed significantly the shape of them, particularly in the post peak section has changed considerably. The tails of the peaks are now much higher and match much better with the experimental results. This change is directly due to the increased volume of water being released into the system by dehydration. The reason that this effect does not significantly change the height of the peaks is that, according to equation (21) and supported by [15], dehydration does not begin until the temperature reaches 200°C. As can be seen from the temperature profiles (Figures 4b, d, f &h) this temperature is not reached until after the peak gas pressures have been passed. Although the gas pressure profiles seem to suggest that the updated dehydration curves offer a better representation of the true volumes of water being introduced into the system, it can also be seen that the temperature profiles are adversely affected. As the volume of water from dehydration increases the temperatures fall and no longer match the experimental temperatures in the latter part of the analyses. This is simply because there is more water in the system to absorb energy through heat capacity

and phase change (evaporation). The solution to this problem may lie with the material properties or, may be a function of the heat and mass transfer through the boundary [3].

Analysis 3 – Gas-slip

Gas-slip is a phenomenon whereby, in contrast to laminar flow of a liquid passed a solid, gases exhibit non-zero flow at the fluid-solid interface. In porous materials like concrete this has been shown to affect the flow rate of gases through the material such that it significantly deviates from macro-scale predictions of Darcian flow behaviour [8]. To account for this behaviour this model uses a formula developed in [8] that introduces a factor, k_g, a function of the Klinkenberg gas-slip flow constant, that increases the permeability for gas flow above that of liquid flow (9). As can be seen this factor is dependent on the intrinsic permeability of the material and the gas pressure. It is therefore variable in a transient problem such as the one studied here and can produce gas permeabilities several orders of magnitude larger than the liquid permeability.

To study the influence of this factor the benchmark analyses conducted in *Analysis 2* were repeated with the gas-slip factor set to 1. Figure 5a shows the result when gas-slip is neglected (cf. Figure 4c). As can be seen the gas pressures are overestimated by a large amount and the numerical analysis failed after approximately 70 mins as 100% saturation with liquid water was reached. Re-tuning these results via permeability (Figure 5b) shows that an order of magnitude reduction can be achieved in the model permeability, bringing it closer to the experimentally measured values (See Figure 2). Figures 5c & d show similar results for B60 concrete, with a 2 order magnitude reduction achieved (cf. Figure 4g). These results suggest that the model for the Klinkenberg constant overestimates the difference between the gas permeability and liquid permeability in these concretes. More work is required to understand why when an additional micro structural mechanism is added to the formulation a poorer correlation is seen with macro-scale results but it may be that gas-slip is not as significant under high temperature conditions.

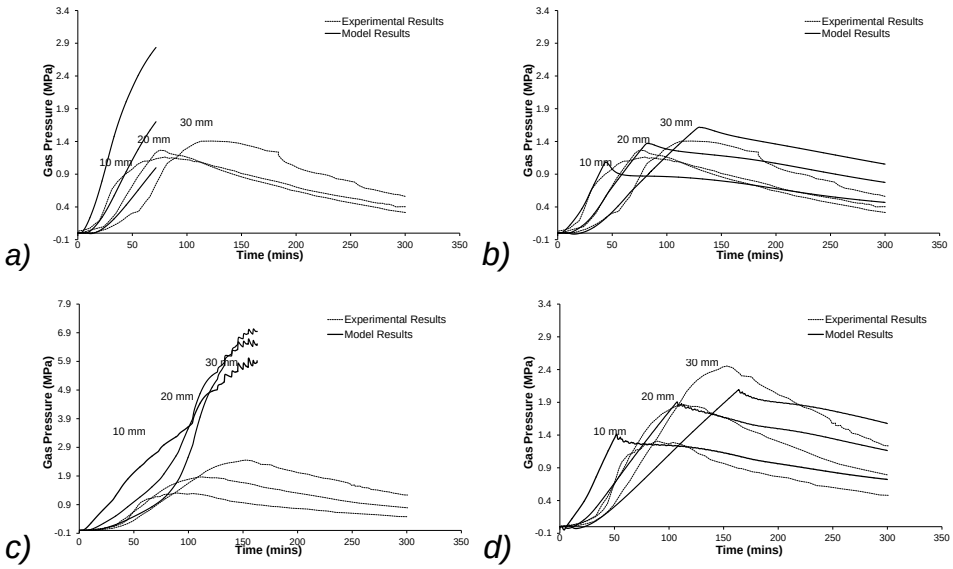

Figure 5 Numerical and experimental results showing gas pressures in time for a) B40 without gas-slip effect K_0=1.0×10^{-19}m^2; b) B40 without gas-slip effect K_0=6.0×10^{-18}m^2; c) B60 without gas-slip effect K_0=6.0×10^{-20}m^2; d) B60 without gas-slip effect K_0=4.0×10^{-18}m^2

Analysis 4 – Evolution of capillary pressure

Another important phenomenon rooted in the micro-structure is capillary pressure, i.e. the difference between the gas and liquid pressures found across capillary menisci that form in the partially saturated porous structure. This micro-scale pressure difference has an effect on the macro-scale pressure gradients that drive fluid flow behaviour. To account for

capillary pressure, the model used here employs Kelvin's equation (12). However, following the work of Gawin et al. [9], the development of capillary pressure is limited to the range above the solid saturation point ($S \geq S_{SSP} = 0.55$) where liquid water exists.

The authors can find no argument to support the assumed value of $S = 0.55$ apparently used by Gawin et al. as a cut-off for capillary menisci and so, to explore the influence of the evolution of capillary pressure in the lower saturation range *Analysis 2* was again re-run, but this time with the solid saturation point set to zero, i.e. with no limit to the development of capillary pressures. Figures 6a & b show the results when the capillary pressures are not limted. As can be seen there is little overall change in the position or height of the pressure peaks when compared to Figures 4c & g. However, a critical difference, most noticeable in Figure 6a, is that the shape of the peaks changes from being a sharp point to a more rounded peak, much more like those seen in the experimental results. This seems contrary to the findings of [11] where capillary pressures were found to have almost no influence on the development of gas pressures in heated concrete. However, in that case very rapid heating took place that led to the development of a steep drying front and almost no areas of lower saturation. By contrast, the relatively slower heating rates applied in this benchmark problem result in a much less steep drying front and a large zone of lower saturation. Thus, the development of capillary pressure and its influence on fluid flow at low saturations has a significant effect on the hygro-thermal behaviour of these concretes and as will be shown, this becomes even more significant when combined with other factors.

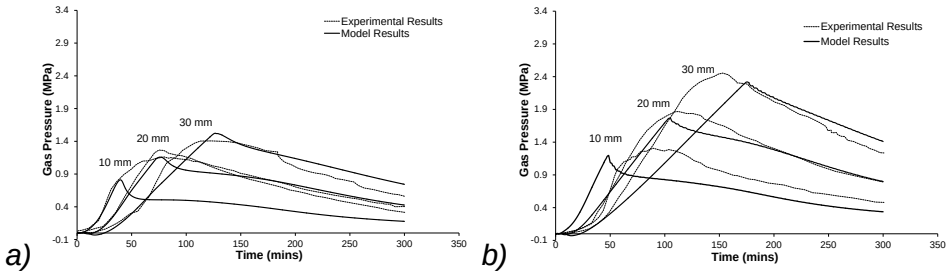

Figure 6 Numerical and experimental results showing gas pressures in time for a) B40 with S_{SSP}=0.0 and b) B60 with S_{SSP}=0.0

Analysis 5 – Combined microstructural considerations

As a final comparison the effects of permeability, dehydration, gas-slip and capillary pressure have been tuned together to give the best fit to the experimental results. As can be seen when Figure 7 is compared to Figure 2, a significant improvement is seen over the original analysis.

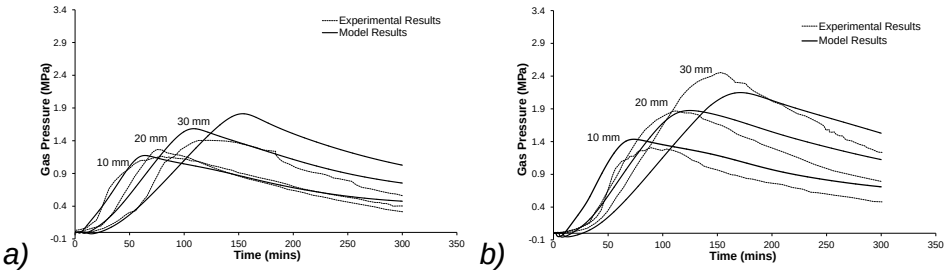

Figure 7 Numerical and experimental results showing gas pressures in time for a) B40 & b) B60 both with $K=3.0\times10^{-18}$ m^2, f_{rec}=0.4, no gas-slip effect and S_{SSP}=0.0

Conclusions

The experimental tests developed and reported in [1] have been employed as a benchmark problem with which to explore numerically the influence of various micro-structural mechanisms on the observed macro-scale behaviour of concrete exposed to elevated

temperatures. Specifically, consideration has been given to intrinsic permeability, the quantity of water recoverable through dehydration of the solid, cement paste skeleton, the difference between the flow of a gas and the flow of a liquid passed a solid surface (gas-slip) and the evolution of capillary pressures, particularly at lower saturation levels.

In considering dehydration of the cement paste, it was found that the amount of water released by dehydration has a significant effect on the shape of the gas pressure peaks. While, due to the temperature regime in this problem, the heights of the peaks (and hence the apparent permeability) were generally unaffected, the post peak pressures were much better matched when larger amounts of water were available through dehydration. However, the addition of this water had a negative effect on matching of the temperature profiles as heat energy was absorbed by heat capacity and phase change. It may be further noted that the release of water from the solid skeleton is directly related to an increase in the micro-structural pore size and therefore, the macro-scale properties of porosity and permeability should be related to dehydration. To address this, the evolution of the pore size distribution with temperature will be further explored.

In considering gas-slip, it was found that it can have a very significant effect on the development of gas pressures in this problem. More work is required to understand if the gas-slip model employed here is specifically unsuitable or if the phenomenon itself is not significant under high temperature conditions. It is clear that for this problem, neglecting gas-slip produces quite different results and moves the predicted permeability one or two orders of magnitude closer to experimentally measured values.

In considering capillary pressures it can be seen that their development and influence on fluid flow at low saturations has a significant effect in this problem and particularlly affects the shape of the gas pressure peaks. It can be further seen that this effect is even more significant when taken in combination with other micro-structural factors. Contrasting with previous work [11], it is clear that they must be taken into account when relatively low heating rates lead to shallow drying fronts and zones of low saturation.

In addition to this, as has been shown before, e.g. [2], intrinsic permeability remains a very significant factor in the development of gas pressures in heated concrete. While improved consideration of the other factors explored here leads to closer alignment with experimentally measured permeabilities there remains a significant difference with numerical values required to match gas pressure results. More work is still required here.

Reference

1. Mindeguia, J.-C., " Numerical Benchmark of experiments on heated concrete", Proceedings of 5th International Workshop on Concrete Spalling due to Fire Exposure. Borås, Sweden, 12-13, September, 2017.
2. Wang, J., Davie, C.T,. Masoero, E., "RILEM TC 256 - Numerical Benchmark of experiments on heated concrete", Proceedings of the 6th International Workshop on Concrete Spalling due to Fire Exposure, 185-196, Borås, Sweden, 12-13, September, 2017.
3. Davie, C.T., Pearce, C.J., and Bićanić, N., "A fully generalised, coupled, multi-phase, hygro-thermo-mechanical model for concrete", *Materials and Structures*, **43**, 13-33, 2010.
4. Taylor, R.L., *FEAP - A Finite Element Analysis Program. Version 8.2 User Manual*, University of California at Berkeley. 2008.
5. Davie, C. T. et al., "Modelling of transport processes in concrete exposed to elevated temperatures – An alternative formulation for sorption isotherms." *Cement and Concrete Research,* **106**, 144-154, 2018.
6. Witek, A. et al., "Finite element analysis of various method for prediction of concrete structures against spalling during fire." *Comput. Mech.* **39**, 271-292, 2005.

7. Tenchev, R. T. and Purnell, P., "An application of a damage constitutive model to concrete at high temperature and prediction of spalling." *International Journal of Solid and Structures*, **42**, 6550-6565, 2005.
8. Chung, J.H., Consolazio, G.R., “Numerical modelling of transport phenomena in reinforced concrete exposed to elevated temperatures”. *Cement and Concrete Research*, **35**,597–608, 2005.
9. Gawin, D., Majorana, C.E., and Schrefler, B.A., “Numerical analysis of hygro-thermal behaviour and damage of concrete at high temperature”, *Mechanics of Cohesive-frictional Materials*, **4**, 37-74, 1999.
10. Cengel, Y.A., *Heat Transfer: A Practical Approach*, Mcgraw-Hill. 2002.
11. Davie, C.T., Pearce, C.J., and Bićanić, N., “Coupled Heat and Moisture Transport in Concrete at Elevated Temperatures—Effects of Capillary Pressure and Adsorbed Water”, *Numerical Heat Transfer, Part A: Applications*, **49**, 733-763, 2006.
12. Tenchev, R.T., et al., “Finite Element Analysis of Coupled Heat and Moisture Transfer in Concrete Subjected to Fire”, *Numerical Heat Transfer: Part A: Applications*, **39**, 685-710, 2001a.
13. Kalifa, P., Menneteau, F.D., Quenard, D., “Spalling and pore pressure in HPC at high temperatures”, *Cement and Concrete Research*, **30**, 1915-1927, 2000.
14. Mounajed, G., Obeid, W., “A New Coupling F.E. Model for the Simulation of Thermal-Hydro-Mechanical Behaviour of Concretes at High Temperatures”, *Materials and Structures* **37**, 422-432, 2004.
15. Dauti, D., et al., "Modeling concrete exposed to high temperature: Impact of dehydration and retention curves on moisture migration." *International Journal for Numerical and Analytical Methods in Geomechanics* 42(13), 1516-1530, 2018.
16. Davie, C. T., et al., "Aspects of Permeability in Modelling of Concrete Exposed to High Temperatures." *Transport in Porous Media,* **95(3)**, 627-646, 2012.
17. Bažant, Z. P. and M. F. Kaplan., Concrete at High Temperatures: Material Properties and Mathematical Models. Harlow, Longman, 1996.
18. Harmathy, T. Z., "Thermal Properties of Concrete at Elevated Temperatures." *ASTM Journal of Materials* **5(1)**, 47-74, 1970.